

Autocatalytic spin-crossover transition: Nonlinear dynamics induced by a photothermal instability

Kamel Boukheddaden,* Miguel Paez-Espejo, François Varret, and Mouhamadou Sy

*Groupe d'Etudes de la Matière Condensée, UMR 8635, CNRS–Université de Versailles Saint-Quentin-en-Yvelines,
45 Avenue des Etats Unis, 78035 Versailles, France*

(Received 20 March 2014; revised manuscript received 5 May 2014; published 23 June 2014)

This predictive theoretical contribution demonstrates that spin-crossover (SC) solids, under light in the regime of the thermally induced hysteresis loop, contain all necessary ingredients for observing autocatalytic behaviors. The sustained oscillations of the high-spin (HS) fraction emerge spontaneously as a result of a subtle balance between the nonlinear relaxation of the HS fraction and the photothermal effect caused by a steady light excitation. Here, we perform a detailed analytical study based on linear stability investigations to clarify the conditions of emergence of such phenomena with respect to the system's parameter in SC solids. Very accurate predictions were obtained and confirmed by the numerical investigations. The treatment developed here should generate experimental results on the nonlinear dynamics and self-induced oscillations in SC solids, and furthermore it should open the perspective of future observations of dissipative structures and pattern formation in all kinds of switchable molecular solids.

DOI: [10.1103/PhysRevB.89.224303](https://doi.org/10.1103/PhysRevB.89.224303)

PACS number(s): 75.30.Wx, 68.35.Rh, 64.60.De

I. INTRODUCTION

Nature shows a tremendous number of examples illustrating nonlinear phenomena drawn from various subjects (mechanics, hydrodynamics, chemistry, population dynamics, life sciences, biology, etc.), demonstrating the universal reach of these behaviors. Thus, one of the most profound and definitive teachings of nonequilibrium thermodynamics relates to the double and ambivalent role of the irreversible processes, which destroy the order near the equilibrium and create the order far from equilibrium. There is, however, no evidence for the existence of a general extrema principle allowing us to predict towards which state a nonequilibrium system is evolving. Contrary to equilibrium states, the evolution of which is moving towards a state minimizing a thermodynamical potential, nonequilibrium states bring elements of unpredictability, even when the equations of motion are known. Indeed, when the thermodynamical branch becomes unstable, several states become accessible. Thus, under the influence of fluctuations or other random factors, the system may evolve towards one state among several others possible. Chemical reactions with proper feedback mechanisms (caused by complex kinetics or thermal effects) may, when maintained far from equilibrium, show multiple stationary states. In particular, when the reactions are coupled with transport processes (e.g., with diffusion), spatial concentration structures may arise [1]. One of the most interesting and intriguing behaviors observed in systems maintained far from equilibrium is the autocatalytic reactions, which have long fascinated physicists and chemists because of their unique features [2]. The situation becomes much more interesting in the presence of many chemical reactions, where one or more reactions produce a catalyst for some of the other reactions. Then the whole collection of constituents is called an autocatalytic set [3]; these constituents have been identified as important processes playing a key role in producing complex or self-replicating molecules, which are required for the origin of life on earth [4–6].

From a general point of view, the buzzword “nonlinearity” is the key feature of several exotic physical phenomena carrying feedback in closed or open systems. Examples are found in the oscillatory and patterned fronts emerging around spontaneous instabilities in phase transitions, when the reactant diffuses much more rapidly than the autocatalyst or heat [7]. Such self-organizations also appear in cardiac arrhythmias [8], where the synchronization of the cardiac cells still attracts a lot of interest. Since the pioneering work of Turing [9], it has been well known that systems showing feedback in situations where not all species diffuse with the same mobility may give rise to spontaneous pattern formation. Interpreted in the language of phase transitions, systems in a situation of instability with enough nonlinear character and subject to several order parameters may show a spontaneous self-organization. In particular, the formation of self-organized localized structures may occur during the dynamics as a result of the autocatalytic behavior. One common aspect of these various features lie in their description with the three classes of models based on reaction-diffusion (RD), Ginzburg-Landau, and Swift-Hohenberg equations. Among these three classes, RD equations were widely used to describe two diffusion equations with source of reactants [10,11].

The source amplitude may increase linearly or nonlinearly with the concentration of one component (activator) and decreases with the other component (inhibitor). In waves of exothermic reaction, the roles of activator and inhibitor are played by heat and reaction products, respectively. Spin-crossover solids [12], which are prototypes of cooperative bistable materials, can be subject to activation and inhibition processes when they are submitted to light, which causes their local heating through a photothermal effect. Light is usually used in these systems to investigate their thermal properties, like in reflectivity measurement [13], UV-VIS spectroscopy [14], or optical microscopy investigations [15], as well as in Atomic Force Microscopy (AFM) [16] and other near-field microscopy measurements. For very small crystals or particles (a few hundred microns), the thermal heating resulting from the presence of light cannot be neglected, so most of these observations should take into account this

*kbo@physique.uvsq.fr

photoheating effect. It is worth noticing that quite recently, experimental evidence of nonlinear behavior of the high-spin (HS) fraction has appeared, such as oscillations of the HS fraction during the photoexcitation and the relaxation processes of spin-crossover microparticles [17]. Furthermore, recent theoretical developments have showed that the propagation of the HS-LS interface during the thermally induced HS to low-spin (LS) transition and vice versa can be described well by an RD equation [18]. In these works, however, only isothermal properties of the front propagation have been considered, and no nonlinear effects have emerged from this description, although it reproduces well the interface propagation process in spin-crossover single crystals.

The theoretical work taking into account the photothermal effects and the subsequent photothermal instability was provided only recently [19]. In that work, we analyzed numerically the various behaviors of the system and found that in some conditions the latter can show sustained oscillations. However, in this preliminary work, we did not establish the general theoretical frame leading to the understanding of the necessary physical conditions to observe nonlinear dynamics effects in spin-crossover (SC) solids under photoexcitation. In the present work, we consider the general behavior of SC solids under light with photoheating, and we develop a general analytical approach to predict a number of nonlinear behaviors, including autocatalytic effects. For the sake of simplicity, we restrict the study to the thermally induced transition, where the quantum yield of the light-induced electronic Franck-Condon transitions between the LS and the HS states is negligible but the photoheating of the sample is not. As a consequence, the theoretical description of the system requires two equations of motion, one on the high-spin fraction (activator) and the other one on the temperature (the inhibitor), which will be explicitly developed in this work.

This paper is organized as follows: in Sec. II, we introduce the generalized master equation approach, and in Sec. III we give the equations of motion of the homogeneous system and perform a linear analysis of the stability in Sec. IV. In Sec. V, we present the time dependences of the HS fraction and temperature, showing the presence of autocatalytic regimes, and in Sec. VI, we conclude.

II. DYNAMICAL ASPECTS OF THE PHOTOTHERMAL INSTABILITY

A huge number of nonequilibrium properties of SC solids have been described within the macroscopic master equation approach [13,14,20]. This equation is based on the homogeneous mean-field approach and involves the time dependence of the net magnetization per site m as function of temperature, interactions, and intrinsic energy barriers in the LS and HS states.

A. Equation of motion of the high-spin fraction

From a microscopic treatment, based on a description of the SC by an Ising-like model, it is straightforward to establish that one of the ways to get the dynamical properties of these systems consists of using a free-energy dynamics to derive the time dependence of the HS fraction (or the net magnetization),

which is then given in the case of a homogeneous system by,

$$\frac{\partial m}{\partial t} = -\frac{\partial \mathcal{F}^{\text{hom}}}{\partial m} = \Gamma J[-m + \tanh \beta(Jm - \Delta_{\text{eff}})], \quad (1)$$

where \mathcal{F}^{hom} is the homogeneous mean-field free-energy whose expression is given in [21], Γ is a phenomenological frequency factor, J is the interaction parameter between the SC units, Δ_{eff} accounts for the effective ligand field energy where $\Delta_{\text{eff}} = \Delta - \frac{1}{2}k_B T \ln g$, Δ is the ligand field energy contribution, g is the degeneracy ratio between the HS and the LS states, k_B is the Boltzmann constant, T is the temperature and $\beta = (k_B T)^{-1}$.

Very recently [18], we extended this approach to include the description of inhomogeneous systems in which the net magnetization is space and time dependent, so that $m(\vec{r}, t)$ represents the spatiotemporal dependence of the net magnetization per site. Expanding the free energy [21] about its homogeneous value of power gradients and assuming an isotropic material lead to the following reaction-diffusion equation:

$$\frac{\partial m}{\partial t} = \Gamma J[-m + \tanh \beta(Jm - \Delta_{\text{eff}})] + D_m \nabla^2 m, \quad (2)$$

in which D_m is the diffusion constant which relates to the second derivative of the free energy with respect to power gradients and Γ is a frequency factor fixing the time scale (which can be temperature dependent), which clearly appears here as a phenomenological parameter. In addition, the coordination number ($z = 4$) is absorbed in the interaction parameter J . We recall that the high-spin fraction n_{HS} is related to m through

$$n_{\text{HS}} = (m + 1)/2. \quad (3)$$

It is important to mention that within the dynamical potential description [20], where the transition rates are of the Arrhenius type, the equation of motion is written

$$\frac{\partial n_{\text{HS}}}{\partial t} = -n_{\text{HS}} K_{\text{HL}} + (1 - n_{\text{HS}}) K_{\text{LH}}, \quad (4)$$

where the expressions of the transition rate K_{HL} (K_{LH}) from HS to LS (LS to HS) are given by $K_{\text{HL}} = k_{\infty} \exp(-\beta E_{\text{HL}}) \exp[-\beta J(n_{\text{HS}} - 1/2)]$ ($K_{\text{LH}} = g k_{\infty} \exp(-\beta E_{\text{LH}}) \exp[\beta J(n_{\text{HS}} - 1/2)]$). Here, E_{HL} and E_{LH} are the intrinsic energy barriers of the noninteracting molecular units. Both descriptions, however, lead to the same self-consistent equation at high temperature. So, for the sake of simplicity, we use here the free-energy dynamics in which the system evolution follows the free-energy landscape.

B. Photothermal effect and equation of motion of temperature

In most of the works dedicated to studying the light-induced effects of SC solids, except for some rare cases [17,19], the thermal effects have been neglected in nonlinear kinetics by anticipating a very efficient energy transfer through an instantaneous heat conduction, ensuring a constant and spatially homogeneous value of the temperature. Whenever these conditions are not satisfied, the temperature can play a very efficient role as a source of oscillation, especially if the system releases heat locally through certain exothermic reactions.

In the following, we discuss the case of one of the first examples of sustained oscillations in a temperature-dependent system that we predicted theoretically but have

not yet revealed experimentally in SC solids. In a recent experimental work [15], we have demonstrated the efficiency of light excitation in controlling the front transition (the HS-LS interface) of a SC solid. It is important to mention here that this effect is purely photothermal due to the fact that the photoinduced processes are operating only at very low temperatures, typically below 90 K.

Let I_o be the intensity of the light used to investigate the spin-crossover properties in reflectivity measurements, optical microscopy, AFM, or other types of experimental setups. Let us denote by a_{LS} (a_{HS}) the optical absorption of the LS (HS) state; usually, we have $a_{HS} < a_{LS}$ because the optical density of the LS state (which is much darker) is higher than that of the HS state. Let n_{HS} be the HS fraction present in the system at time t and temperature T ; then the heating effect induced by the light intensity can be considered to be simply proportional to the fractions of the HS and LS species in the system, i.e., $I_o[a_{LS}(1 - n_{HS}) + a_{HS}n_{HS}]$. The second source of heat comes for the enthalpy variation ΔH accompanying the LS \leftrightarrow HS change, whose contribution depends on the transformation rate as $-\frac{\Delta H}{C_p} \frac{\partial m}{\partial t}$, where C_p is the specific heat. Finally, the interaction between the spin-crossover crystal maintained at temperature T and the thermal bath, with a temperature $T_B < T$, tends to cool down the crystal, thus introducing another contribution, $-\alpha(T - T_B)$, to the temperature flow, where α is the cooling coefficient. Then, the balance of the heat (giving the evolution of temperature), including the previously mentioned contributions and thermal diffusion, is written as

$$\begin{aligned} \frac{\partial T}{\partial t} = & -\alpha(T - T_B) - \frac{\Delta H}{C_p} \frac{\partial m}{\partial t} \\ & + \frac{I_o a_{LS}}{C_p} \frac{M}{m_a} \left(1 + (\rho - 1) \frac{1 + m}{2} \right) + D_T \nabla^2 T, \end{aligned} \quad (5)$$

where C_p is the system heat capacity given in $\text{J K}^{-1} \text{mol}^{-1}$, $\rho = \frac{a_{HS}}{a_{LS}} < 1$ is the ratio between the absorption coefficients of the HS and LS states, m_a is the sample mass, M is its molar mass, and $D_T \nabla^2 T$ relates to thermal diffusion, with a diffusion constant D_T . For the sake of simplicity, the product $\frac{I_o a_{LS}}{C_p} \frac{M}{m_a}$ will hereafter be denoted I .

Equations (2) and (5) form a set of nonlinear coupled partial derivative equations describing the spatiotemporal properties of a SC system under photothermal effects. In the next section, we will consider spatially uniform systems and study situations where the equations of evolution admit more than one steady state.

C. On the choice of the parameter values

Hereafter, we choose the realistic parameter values, derived from optical microscopy experiments [15] on the SC single crystal $[\text{Fe}(\text{NCSe})(\text{py})_{22}(\text{m-bppyz})]$, where py = pyridine and bppyz = 3,5-bis(2-pyridyl)-pyrazolate [22], hereafter abbreviated Fe(NCSe). For this system, we have $J = 152 \text{ K}$ for the interaction between the spin states, $\Gamma = 0.5 \text{ K}^{-1} \text{ s}^{-1}$, $\Delta = 394 \text{ K}$ for the ligand field, $\ln g = 7$ for the logarithm of the degeneracy ratio (leading to an entropy change at the transition, $\Delta S = R \ln g \simeq 57 \text{ J K}^{-1} \text{ mol}^{-1}$), and a transition

temperature (also called the equilibrium temperature)

$$T_{eq} = \frac{2\Delta}{k_B \ln g} \quad (6)$$

of 112.6 K. The corresponding enthalpy change is then $\Delta H = T_{eq} \Delta S \sim 6340 \text{ J mol}^{-1}$. The single crystals of Fe(NCSe) have a molar mass $M = 880 \text{ g mol}^{-1}$. Those used in optical microscopy experiments have a typical size $400 \mu\text{m} \times 20 \mu\text{m} \times 10 \mu\text{m}$ (volume $V = 8 \times 10^{-8} \text{ cm}^3$), their density is around $d = 1.5 \text{ g cm}^{-3}$, and their associated specific heat at the transition is $C_p \simeq 176 \text{ J K}^{-1} \text{ mol}^{-1}$. The heat of the reaction associated with such a single crystal (assuming a total change from LS to HS) is then easily evaluated as equal to $\frac{\Delta H d V}{M} \simeq 10^{-7} \text{ J}$. Equation (1) shows that, in the homogeneous case ($D_m = 0$) and around the transition temperature, $\Delta_{\text{eff}} = 0$, it is quite easy to demonstrate that $\frac{\partial m}{\partial t} \simeq \Gamma J (\beta_{\text{eq}} J - 1) m$, where m takes small values around zero. Inserting this contribution in the equation of evolution of temperature leads to an additional source term which plays the same role as photoheating [because $(1 - \rho) < 0$]. However, since we are mainly interested in the photothermal effects and for the sake of simplicity, we will not consider this term in this study; its role in the general case will be investigated in a future work. Now, we turn to the evaluation of the photoheating part. $\alpha = 2.0 \text{ s}^{-1}$ is a typical value of the thermal coupling time of the crystal to the thermal bath, in other words, the response time (0.5 s) under vacuum to an instantaneous change in the shining power, determined by suited (unpublished) optical microscopy experiments. The usual optical microscopy measurements allowing us to follow the spatiotemporal aspects of SC solids are performed with a specific intensity $I_s \sim 50 \text{ mW/cm}^2$. So the power received by the crystal is $P = a I_s S \simeq 1.6 \mu\text{W}$, where a ($a_{LS} \sim 0.4$ and $a_{HS} \sim 0.2$) is the optical absorption of the crystal and $S = 8000 \mu\text{m}^2$ is its surface ($a I_s = I_o$). This results in a contribution to the crystal temperature change [given by Eq. (5)] of $I = \frac{a I_s S M}{C_p d V} \simeq 66 \text{ K s}^{-1}$, which is two times bigger than the contribution of the enthalpy of the reaction, which is omitted in the investigations presented in this work.

III. HOMOGENEOUS SYSTEM

Based on the previous discussion, we investigate the nonequilibrium thermodynamics of the homogeneous system for which, obviously, we neglect the diffusion terms in both Eqs. (2) and (5). The physical system is then described by the following equations of motion:

$$\frac{\partial m}{\partial t} = \Gamma J [-m + \tanh \beta (Jm - \Delta_{\text{eff}})], \quad (7)$$

$$\frac{\partial T}{\partial t} = -\alpha(T - T_B) + I \left(1 + (\rho - 1) \frac{1 + m}{2} \right). \quad (8)$$

The equations of the stationary states are given by setting $\frac{\partial m}{\partial t} = \frac{\partial T}{\partial t} = 0$ in Eqs. (7) and (8), which leads to

$$m_0 = \tanh \beta_0 (Jm_0 - \Delta_{\text{eff}}), \quad (9)$$

$$T_0 = T_B + \frac{I}{2\alpha} [\rho + 1 + m_0(\rho - 1)], \quad (10)$$

where $\beta_0 = (k_B T_0)^{-1}$ and, obviously, $T_0 > T_B$.

Here, we are mainly interested in the dynamic properties of the system inside the hysteresis loop, that is, the bistable region. To make the analytical developments easier, we chose to work around the transition temperature T_{eq} [given by Eq. (6)] at which $m_0 = 0$ and for which it corresponds to the intensity I_{eq} , given by

$$I_{eq} = \frac{2\alpha}{\rho + 1}(T_{eq} - T_B). \quad (11)$$

Injecting relation (11) in (10) leads to the simple stationary temperature,

$$T_0 = T_{eq} - \gamma(T_{eq} - T_B)m_0, \quad (12)$$

where, for the sake of simplicity, we define $\gamma = \frac{1-\rho}{1+\rho}$. Relation (12) has to be used with Eq. (9) in order to explore the thermodynamical properties of this system under light. In Fig. 1 we show the temperature dependence of the HS fraction for both stationary solutions given in Eqs. (9) and (12) for different values of the photoexcitation's intensity, $I = I_{eq}$ [whose expression is given by Eq. (11)]. The latter can be monitored by changing the bath temperature T_B . We have considered here the situation where the thermal dependence of the HS fraction, resulting from Eq. (9), leads to a thermal hysteresis loop, a behavior which is possible only if we fulfill the condition $(\beta_{eq}J - 1) > 0$, as already reported several times in the literature. So, in this situation, the system admits an unstable branch, which is easily identified since it is characterized by $\frac{\partial n_{HS}}{\partial T} < 0$. We will see later that this condition is an essential prerequisite for the emergence of spontaneous nonlinear dynamics under light. One can remark in Fig. 1 that according to I_{eq} values, the system transforms from monostable to bistable when the equilibrium intensity is below

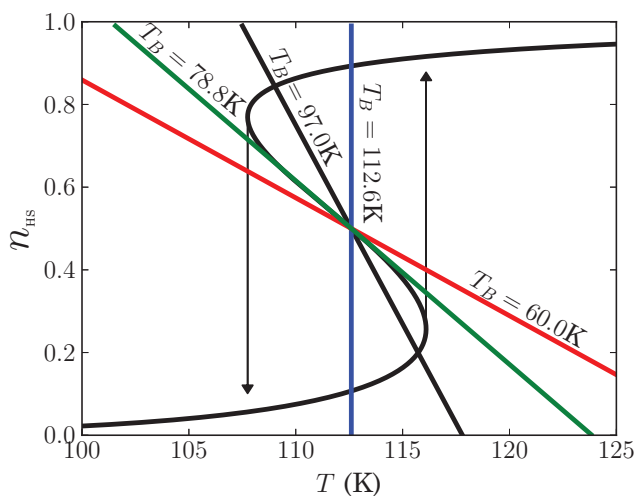


FIG. 1. (Color online) The black line shows the thermal hysteresis loop arising from the mean-field analysis of the homogeneous system. The colored lines correspond to the HS fraction dependence of the systems' temperature for various values of the bath temperature, $T_B = 112.6 (=T_{eq})$, 97.0 , $78.8 (=T_B^{\text{crit}})$, and 60.0 K, corresponding to I_{eq} values of 0 , 41.6 ($2.17 \mu\text{W}$), 90 ($4.7 \mu\text{W}$), and 140 K s^{-1} ($7.3 \mu\text{W}$), respectively. The other parameter values are as follows: $J = 152 \text{ K}$, $\Delta = 394.1 \text{ K}$, $\ln g = 7$, $\rho = 0.5$, $\alpha = 2.0 \text{ s}^{-1}$, $D_m = D_T = 0$.

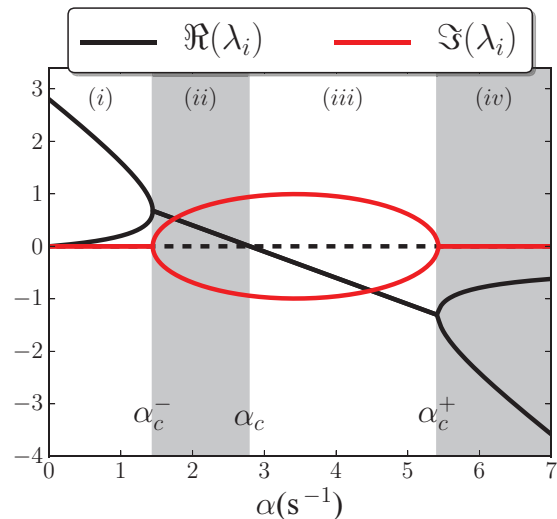


FIG. 2. (Color online) Dependence of the real (black curve) and the imaginary (red curve) parts of the eigenvalues on the parameter α , which represents the thermal coupling between the system and the reservoir. Several regions emerge and correspond to different expected dynamical behaviors of the system. See text for further explanation. Parameter values are $\Gamma = 1/19.0 \text{ K}^{-1} \text{ s}^{-1}$, $J = 152 \text{ K}$, $\ln g = 7$, $\rho = 0.5$, $T_B = 75 \text{ K}$, $T_{eq} = 112.6 \text{ K}$, and $\Delta = 394 \text{ K}$.

the critical value,

$$I_{eq}^{\text{crit}} = 4\alpha \frac{J - k_B T_{eq}}{(1 - \rho)k_B \ln g}, \quad (13)$$

which is obtained from Eqs. (9) and (10) by comparing the slopes of the corresponding $m(T)$ curves (see Fig. 1) when $m = 0$. Using the parameter values given in the caption of Fig. 1, expression (13) leads to $I_{eq}^{\text{crit}} \simeq 90 \text{ K s}^{-1}$ ($4.7 \mu\text{W}$). In Fig. 2, I_{eq} was monitored by varying the T_B values,

$$T_B^{\text{crit}} = T_{eq} \left(1 - 2 \frac{\beta_{eq} J - 1}{\gamma \ln g} \right), \quad (14)$$

and the critical bath temperature corresponding to the critical intensity value below which the system shows a single fixed point is given by $T_B^{\text{crit}} \simeq 78.8 \text{ K}$. Hereafter, we study the case of one fixed point, corresponding to $I > I_{eq}^{\text{crit}}$ and $T_B < T_B^{\text{crit}}$.

IV. LINEAR ANALYSIS OF THE STABILITY

To investigate the nonequilibrium properties of Eqs. (7) and (8), we first perform a linear analysis of the stability to get the global tendencies. Around the stationary states, m_0 and T_0 , the variables m and T can be written $m = m_0 + \delta m(t)$ and $T = T_0 + \delta T(t)$, where $\delta m(t)$ and $\delta T(t)$ are small perturbations. Simple mathematical developments show that the previous system becomes

$$\frac{d\vec{x}}{dt} = \Lambda \vec{x}, \quad (15)$$

where the vector $\vec{x} = (\delta m(t), \delta T(t))$ and the matrix Λ is the Jacobian of the system of Eqs. (7) and (8), which is written as

$$\Lambda = \begin{pmatrix} \Lambda_{11} & \Lambda_{12} \\ \Lambda_{21} & \Lambda_{22} \end{pmatrix} = \begin{pmatrix} \left. \frac{\partial f}{\partial m} \right|_0 & \left. \frac{\partial f}{\partial T} \right|_0 \\ \left. \frac{\partial g}{\partial m} \right|_0 & \left. \frac{\partial g}{\partial T} \right|_0 \end{pmatrix}, \quad (16)$$

where the expressions of the functions $f(m, T)$ and $g(m, T)$ are given by

$$f(m, T) = \Gamma J[-m + \tanh \beta(Jm - \Delta_{\text{eff}})], \quad (17)$$

$$g(m, T) = -\alpha(T - T_B) + I_{eq} \left(1 + (\rho - 1) \frac{1+m}{2} \right). \quad (18)$$

The subscript 0 indicates that the derivatives are taken around the stationary states ($m_0 = 0$ and $T_0 = T_{eq}$). The elements of the Jacobian Λ are given by

$$\begin{aligned} \left. \frac{\partial f}{\partial m} \right|_0 &= \Lambda_{11} = \Gamma J(\beta_{eq} J - 1), & \left. \frac{\partial f}{\partial T} \right|_0 &= \Lambda_{12} = \frac{\Gamma J \ln g}{2T_{eq}}, \\ \left. \frac{\partial g}{\partial m} \right|_0 &= \Lambda_{21} = -\alpha \gamma(T_{eq} - T_B), & \left. \frac{\partial g}{\partial T} \right|_0 &= \Lambda_{22} = -\alpha. \end{aligned} \quad (19)$$

The characteristic equation of the previous system is written $\text{Det}[\Lambda - \lambda \mathbb{I}] = 0$, where λ are the eigenvalues of the Jacobian matrix. They satisfy the relation

$$\lambda^2 - (\Lambda_{11} + \Lambda_{22})\lambda + \Lambda_{11}\Lambda_{22} - \Lambda_{12}\Lambda_{21} = 0. \quad (20)$$

The expressions of the two eigenvalues λ_1 and λ_2 are

$$\lambda_{\pm} = \frac{(\Lambda_{11} + \Lambda_{22}) \pm \sqrt{D_{\lambda}}}{2}, \quad (21)$$

where

$$D_{\lambda} = (\Lambda_{11} - \Lambda_{22})^2 + 4\Lambda_{12}\Lambda_{21}. \quad (22)$$

According to the Jacobian element values, the discriminant D_{λ} has the expression

$$D_{\lambda} = [\Gamma J(\beta_{eq} J - 1) + \alpha]^2 - 2\alpha \frac{\Gamma J \ln g}{T_{eq}} \gamma(T_{eq} - T_B), \quad (23)$$

which can be written as $D_{\lambda} = (\alpha - \alpha_c^-)(\alpha - \alpha_c^+)$, where the expressions of the critical values α_c^{\pm} are given in Eq. (A1). For the values of Fig. 2, $\alpha_c^- = 1.44 \text{ s}^{-1}$ and $\alpha_c^+ = 5.41 \text{ s}^{-1}$, corresponding to thermal relaxation times of ~ 0.7 and $\sim 0.2 \text{ s}$, respectively.

The sum S and the product P of the two eigenvalues correspond respectively to the trace and the determinant of Λ and are given by

$$S = \lambda_+ + \lambda_- = \Lambda_{11} + \Lambda_{22} = \text{Tr}(\Lambda) \quad (24)$$

and

$$P = \lambda_+ \lambda_- = \Lambda_{11}\Lambda_{22} - \Lambda_{12}\Lambda_{21} = \text{Det}(\Lambda), \quad (25)$$

which are expressed as functions of the model parameters as follows:

$$S = \Gamma J(\beta_{eq} J - 1) - \alpha, \quad (26)$$

$$P = \alpha \Gamma J \frac{2T_{eq}}{\gamma \ln g} (T_B^{\text{crit}} - T_B). \quad (27)$$

In Fig. 2, we have summarized the α dependence of the real and imaginary parts of the two eigenvalues λ_{\pm} , given by Eqs. (21), (22), and (23). The study of the signs of S and P

allows us to classify the singular points. The solutions of the differential equation have the form

$$\delta m(t) = c_1 e^{\lambda_+ t} + c_2 e^{\lambda_- t}, \quad \delta T(t) = c_3 e^{\lambda_+ t} + c_4 e^{\lambda_- t}. \quad (28)$$

From these expressions one also obtains straightforwardly the following stability criteria:

(1) If both $\text{Re}(\lambda_i) < 0$, the steady state (m_0, T_0) is asymptotically stable. This case is represented by regions (iii) and (iv) of Fig. 2, where the black curve (the red curve) is the real part (the imaginary parts) of λ_{\pm} .

(2) If for at least one of the roots $\text{Re}(\lambda_i) > 0$, the state (m_0, T_0) is unstable. This corresponds to regions (i) and (ii) of the phase diagram in Fig. 2. One can easily see from Eqs. (19) that this inequality is realized only if $\Gamma J(\beta_{eq} J - 1) > 0$, which is also the condition to fulfill in Eq. (9) to obtain a thermal hysteresis loop.

(3) If for at least one of the roots $\text{Re}(\lambda_i) = 0$ while the others remain negative, the system is stable in the sense of Lyapunov but is not asymptotically stable.

Once again, once the dependence of $S = \text{Tr}(\Lambda)$ and $P = \text{Det}(\Lambda)$ on the parameters is specified [see Eqs. (24) and (25)], it is immediately possible to see which situation is realized. In addition, from Eqs. (28) we can determine how the perturbed system evolves back or departs from the singular point.

V. ON THE SPONTANEOUS EMERGENCE OF AUTOCATALYTIC OSCILLATIONS IN SC SOLIDS

Here, we analyze the time dependence of the HS fraction and the temperature for the various situations mentioned in the last section. For that we solve numerically the equations of motion (7) and (8) and discuss the results in relation to the predictions derived for the linear stability in the previous section.

A. Both roots are real

When $D_{\lambda} > 0$, both eigenvalues are strictly real, which implies the conditions $\alpha < \alpha_c^-$ [region (i) in Fig. 2] and $\alpha > \alpha_c^+$ [region (iv) in Fig. 2], and the α dependence of the two eigenvalues are given by the following expressions:

$$\begin{aligned} \lambda_{\pm}(\alpha) &= \frac{1}{2} [\Gamma J(\beta_{eq} J - 1) - \alpha] \\ &\pm \sqrt{\frac{[\Gamma J(\beta_{eq} J - 1) + \alpha]^2}{4} - \alpha \frac{\Gamma J \ln g}{2T_{eq}} \gamma(T_{eq} - T_B)}. \end{aligned} \quad (29)$$

If, in addition, $P \equiv \text{Det}(\Lambda) > 0$, which corresponds to $T_B < T_B^{\text{crit}}$ ($= 78.8 \text{ K}$), then the eigenvalues λ_+ and λ_- have the same sign, as we can observe in Fig. 2. According to Eq. (28), this implies a nonoscillatory approach to (or a departure from) the singular point. We obtain in this case a stable ($\lambda_{\pm} < 0$; see Fig. 3) or an unstable ($\lambda_{\pm} > 0$; see Fig. 4) node, which corresponds to regions (i) and (iv) in Fig. 2. Figure 4 depicts the temporal evolution of the HS fraction and temperature for $\alpha = 0.2 \text{ s}^{-1}$ [corresponding to region (i) in Fig. 2, where both eigenvalues are positive], deduced from the numerical resolution of the differential equations (7) and (8). The periodic behavior of $n_{\text{HS}}(t)$ and $T(t)$ leading to a limit cycle in the phase

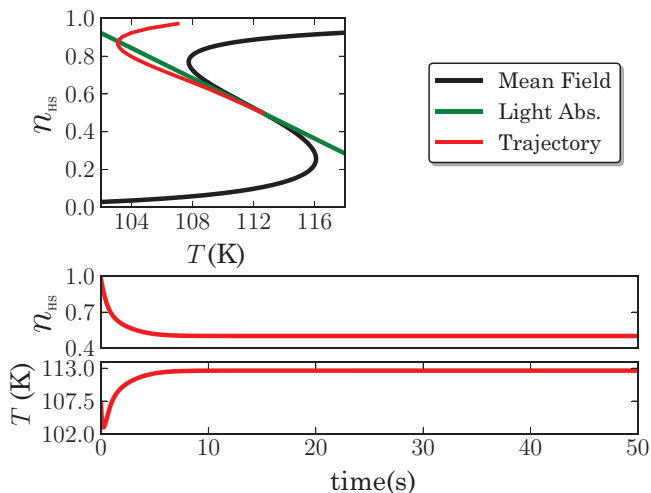


FIG. 3. (Color online) (top) Portrait of the time evolution of the system in the $n_{\text{HS}}-T$ plane in the case where the two eigenvalues of the Jacobian matrix are negative, leading to a stable focus [region (iv) in Fig. 2]. (bottom) Time dependence of n_{HS} and T showing a nonoscillatory approach to the stable fixed point ($n_{\text{HS}} = 1/2$, $T = T_{\text{eq}}$). Initial values were $n_{\text{HS}} = 0.9$, $T = 107.5$ K [$> T_B^{\text{crit}} (=78.8$ K)]. The stationary solutions are shown as guidelines. Parameter values are the same as those in Fig. 2, except $\alpha = 6.0$ s $^{-1}$.

space $n_{\text{HS}} - T(t)$ contrasts with the linear stability analysis, which predicts an exponential growth of the perturbation, which is clearly not adapted far from $m = 0$ ($n_{\text{HS}} = 0.5$), where nonlinear contributions cannot be neglected and even become dominant. In this case, the exponential growth of the

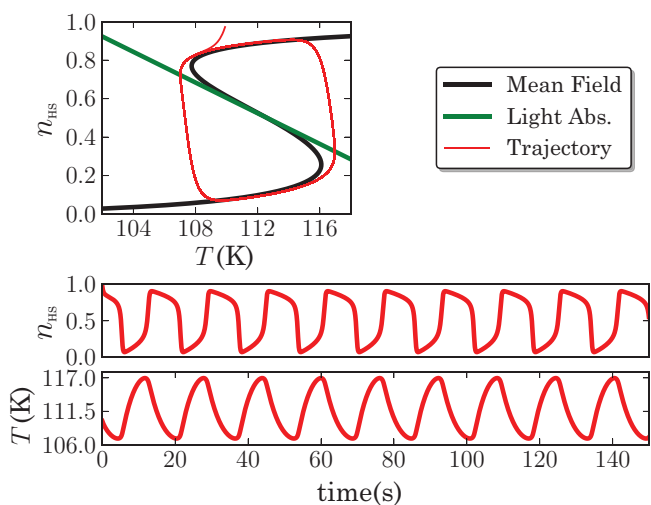


FIG. 4. (Color online) (top) Portrait of the time evolution of the system in the $n_{\text{HS}}-T$ plane showing a limit cycle in the case where the two eigenvalues of the Jacobian matrix are positive, leading to an unstable focus [region (i) in Fig. 2]. (bottom) Time dependence of n_{HS} and T showing nonlinear but periodic oscillations, arising from the numerical resolution of Eqs. (7) and (8). The coordinates of the initial state are $n_{\text{HS}} = 0.9$, $T = 110.0$ K. The stationary solutions are shown as guidelines. Parameter values are the same as those in Fig. 3, except $\alpha = 0.2$ s $^{-1}$.

perturbation will be stopped by the action of the nonlinear terms ($\propto m^3$ at second order), which will drive the system from an unstable state to a steady state.

In the other case, $P \equiv \text{Det}(\Lambda) < 0$, i.e., for $T_B > T_B^{\text{crit}}$, the two real λ_{\pm} roots have different signs. We will obtain in this case a three-fixed-point system like the one shown in Fig. 1 for $T_B > T_B^{\text{crit}}$.

B. Both roots are complex

This situation appears when $D_{\lambda} < 0$ (which implies $\alpha_c^- < \alpha < \alpha_c^+$) is satisfied. This range of values for α corresponds to regions (ii) and (iii) in the phase diagram in Fig. 2, where the red curves are the imaginary parts of the eigenvalues.

The real and complex parts of the two eigenvalues involved are given by

$$\begin{aligned} \text{Re}(\lambda_{\pm}) &= \frac{1}{2}[\Gamma J(\beta_{\text{eq}} J - 1) - \alpha], \\ \text{Im}(\lambda_{\pm}) &= \pm \sqrt{\frac{\alpha \Gamma J \ln g}{2T_{\text{eq}}} \gamma(T_{\text{eq}} - T_B) - \frac{[\Gamma J(\beta_{\text{eq}} J - 1) + \alpha]^2}{4}}. \end{aligned} \quad (30)$$

In this case, the black curve in Fig. 2, representing the real part of the eigenvalues, behaves linearly with α , in agreement with the analytical expression $\text{Re}(\lambda_i) = \Gamma J(\beta_{\text{eq}} J - 1) - \alpha$.

If, in addition, $S \equiv \Gamma J(\beta_{\text{eq}} J - 1) - \alpha \neq 0$, then the two roots have nonvanishing real parts. According to Eq. (28), this implies an oscillatory departure from [$S > 0$ or $\text{Re}(\lambda_i) > 0$] or approach ($S < 0$ or $\text{Re}(\lambda_i) < 0$) to the singular point ($n_{\text{HS}} = \frac{1}{2}$, $T = T_{\text{eq}}$), as depicted respectively in Figs. 5 and 6 [obtained in region (ii) for $\alpha = 2.5$ s $^{-1}$ using different initial conditions] and Fig. 7 [obtained in region (iii) for $\alpha = 3$ s $^{-1}$]. In this case,

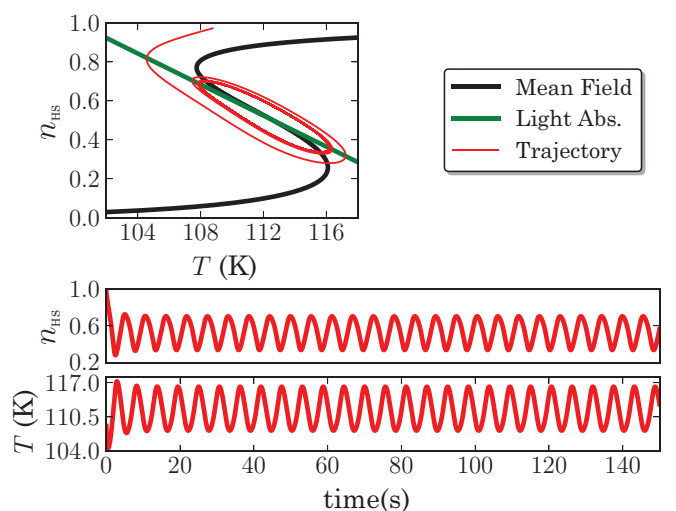


FIG. 5. (Color online) (top) Portrait of the time evolution of the system in the $n_{\text{HS}}-T$ plane in the case where the roots are complex with a positive real part [region (ii) in Fig. 2], leading to an unstable focus and a limit cycle. The initial coordinates are $n_{\text{HS}} = 0.95$ and $T = 108.5$ K. The stationary solution (black and green curves) are shown as guidelines. (bottom) Time dependence of n_{HS} and T showing autocatalytic oscillations. Parameter values are the same as those in Fig. 3, except $\alpha = 2.5$ s $^{-1}$.

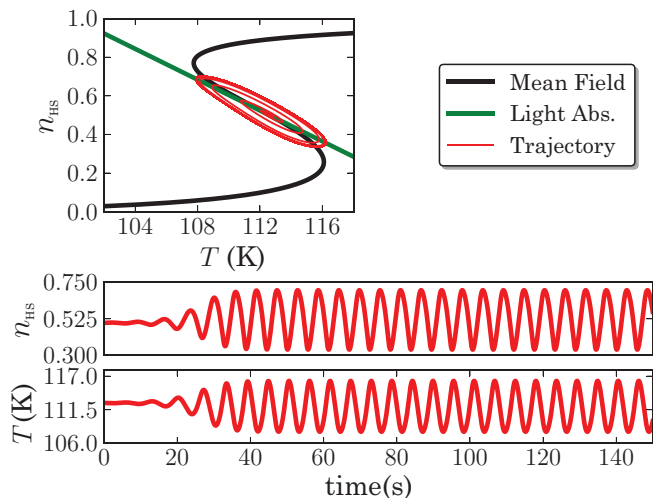


FIG. 6. (Color online) Temporal evolution of the system in the phase space $n_{\text{HS}}-T$ in the case of an unstable focus, starting at time $t = 0$ s from the coordinates $(n_{\text{HS}} = 0.5, T = T_{eq} + \epsilon = 112.61 \text{ K})$. The stationary solutions are shown as guidelines. After a stationary period, the system starts to oscillate around the unstable focus, which describes a stable limit cycle. Parameter values are the same as those in Fig. 5.

the respective stationary solution is called an unstable or a stable focus. The trajectories corresponding to this case are spirals which enter the stationary state (see Figs. 5 and 7) or depart from the stationary state (compare Fig. 6). To check the stability of the obtained limit cycle of Fig. 5, we have restarted the system (at time $t = 0$) from the values $n_{\text{HS}} = 0.5$ and $T = T_{eq} + \epsilon = 112.61 \text{ K}$, which are very close to the coordinates

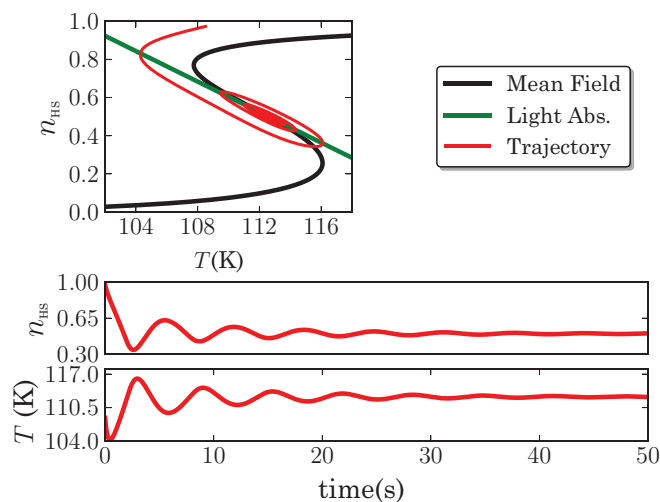


FIG. 7. (Color online) (top) Portrait of the time evolution of the system in the $n_{\text{HS}}-T$ plane in the case where the roots are complex with a negative real part [region (iii)], which leads to a stable focus. The initial coordinates are $n_{\text{HS}} = 1$ and $T = 108 \text{ K}$. The stationary solutions (black and green curves) are shown as guidelines. (bottom) Time dependence of n_{HS} and T showing damped oscillations. Parameter values are the same as in Fig. 3, except $\alpha = 3.0 \text{ s}^{-1}$.

of the unstable focus $(0.5, 112.6 \text{ K})$. Its temporal evolution, presented in Fig. 6, first shows a transitional period of 20 s during which the HS fraction and the temperature are almost constant or weakly fluctuating; then, suddenly, the amplitude of the oscillations increases until it reaches, at $t \simeq 30 \text{ s}$, a stationary state, characterized by a well-defined frequency and amplitude.

C. Critical values and the properties of the limit cycles

To visualize the existence of bifurcation phenomena, we have drawn in Fig. 2 the eigenvalues λ_{\pm} against the control parameter α (it is also possible to do this with T_B or another parameter of the model). There are four regions, denoted (i), (ii), (iii), and (iv), as already discussed, which implies three critical values, α_c^{\pm} and α_c , corresponding to the respective situation where $D_{\lambda} = 0$ and $\text{Re}(\lambda_{\pm}) = 0$. At these points, a bifurcation phenomenon occurs. Then the behavior of the system can be analyzed as a function of the cooling parameter α .

When $S = 0$, i.e., $\text{Re}(\lambda) = 0$ but $P > 0$, which happens at some critical value of α ,

$$\alpha_c = \Gamma J(\beta_{eq} J - 1), \quad (31)$$

with the condition that $T_B < T_B^{\text{crit}}$, the roots become purely imaginary, $\lambda_{\pm} = \pm i\omega$. Within the parameter values used in Fig. 2, $\alpha_c \sim 2.8 \text{ s}^{-1}$ is the α value separating regions (ii) and (iii). In this case, the system's behavior in the phase space is represented by closed trajectories surrounding the singular point, referred to as a center. They represent a system which undergoes sustained oscillations, provided, of course, linearization constitutes a valid approximation. The singular point exhibits the so-called Lyapunov stability, although neither the singular point nor the orbits are asymptotically stable.

In the following, we quote the different cases near α_c :

(1) When $\alpha > \alpha_c = 2.8 \text{ s}^{-1}$, the system admits a negative real-part solution, as already presented in the previous sections. The singular point is then a stable focus, and the trajectory is a spiral entering the stationary state. Over time, we get damped oscillatory solutions (see Figs. 3 and 7), the amplitude of which decreases exponentially, $e^{-\sigma t}$, with a relaxation time $\sigma = -\text{Re}(\lambda_{\pm})$, whose expression can straightforwardly be written as

$$\sigma \propto (\alpha - \alpha_c). \quad (32)$$

In order to test this theoretical prediction, we have carried out numerical simulations by solving the set of two coupled differential equations [(7) and (8)] for $\alpha > \alpha_c$ and have determined from the time dependence of the HS fraction (and temperature), which showed damped oscillations, the damping factor σ , which has been drawn as function of α in Fig. 8. The obtained results show a linear plot of $\sigma(\alpha)$, in excellent agreement with the theoretical predictions of Eq. (32).

(2) For $\alpha < \alpha_c$ the real part of the two eigenvalues is positive, and the solution becomes an unstable focus, around which the trajectories describe a limit cycle (compare Figs. 4 and 5). The amplitude A_n of the oscillations (the size of the

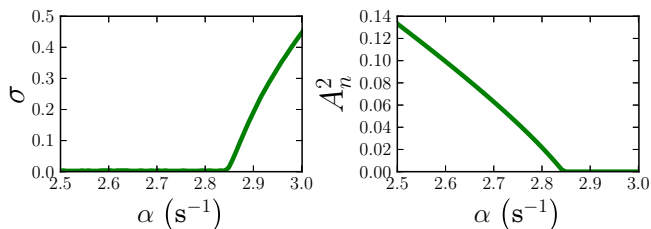


FIG. 8. (Color online) Dependence of the relaxation time σ and the amplitude of oscillations A on the thermal coupling between the SC solid and its surrounding bath α . A critical behavior obeying Eqs. (32) and (33) is obtained. Parameter values are the same as those in Fig. 2

limit cycle) undergoes a critical behavior,

$$A_n \propto \sqrt{\alpha - \alpha_c}, \quad (33)$$

while the frequency is independent of α . In this specific case, the period τ of the oscillations is that obtained for the value $\alpha = \alpha_c$. As a result, we calculate the eigenvalue in this specific situation. Remarking that, at $\alpha = \alpha_c$, we have $\Lambda_{11} + \Lambda_{22} = 0$, the characteristic equation becomes $\lambda^2 + \Lambda_{11}\Lambda_{22} - \Lambda_{12}\Lambda_{21} = 0$, which gives the expression of the period of the limit cycles as $\tau = \frac{2\pi}{\sqrt{\Lambda_{22}^2 - \Lambda_{12}\Lambda_{21}}}$. Replacing the different elements of the Jacobian by their expressions, one gets the expression

$$\tau = \frac{2\pi}{\alpha_c \sqrt{1 + \frac{T_{eq} - T_B}{T_{eq} - T_B^{\text{crit}}}}}, \quad (34)$$

which gives $\tau = 1.54$ s for the parameter values used Fig. 2. This value of the oscillation period is in excellent agreement with the thermal relaxation times (several seconds) fixing the time scale of the coupling between the SC single crystals and the thermal bath.

Figure 8, in which we plot the α_c dependences of σ and A , summarizes the previously obtained results. Clearly, the simulations are in excellent agreement with the predictions of the linear stability analysis, which reproduces quantitatively the numerical data.

(3) For $\alpha = \alpha_c = \Gamma J(\beta_{eq} J - 1)$, the real part of the eigenvalues becomes equal to zero, and only imaginary solutions remain, giving rise to a marginal stable state in which the system oscillates at the frequency $|\text{Im}(\lambda_{\pm})|$. The amplitude of the oscillations is then invariant (at second order) and is fixed by the initial conditions.

VI. CONCLUSION

We have presented a predictive theoretical work showing that the time evolution of the HS fraction of a SC single crystal or particle under light causing photoheating can result in nonlinear dynamics behavior, such as autocatalytic oscillations. The self-oscillations are distinct from resonant systems (including both forced and parametric resonators), in which the oscillation is driven by a source of power which is modulated externally. In the present situation, spontaneous

oscillations of the system are obtained with a source of power that lacks a corresponding periodicity. Indeed, only a self-oscillator can generate and maintain a regular periodicity without requiring a similar external periodicity to drive it. In the present case, we show that a steady intensity signal can generate sustained oscillations in spin-crossover solids in some specific situations that we have analyzed in detail. We found that the control of the intensity of light or the coupling between the thermal bath and the sample (cooling factor here) may induce bifurcations as well as critical phenomena on the amplitude of the oscillations of the HS fraction. Resonant oscillations have recently been observed experimentally [17] on SC microparticles under illumination around the thermally induced hysteresis region of the SC system, through the time dependence of the reflectivity signal, but they are not autocatalytic oscillations, which are still highly desired in this field. Since, in general, the possibility of spontaneous oscillations is diagnosed as an instability of the linearized equations of motion for perturbations about an equilibrium, the latter is usually caused by the presence of a positive feedback between the oscillator “motion” and the power source. In this work, we provided a general and detailed analysis of the prerequisite conditions for observing these nonlinear phenomena in SC materials. In particular, we demonstrate that the presence of a bistability (i.e., a thermally or optically induced hysteresis loop) is an unavoidable condition for observing such autocatalytic behaviors. Several switchable molecular systems, among them Jahn-Teller switches, Prussian blue analogs, and organic bistable crystals, are then possible candidates for observing these nonlinear dynamics. As a consequence, these behaviors are not expected in noncooperative solids. Further extensions of this work to nonhomogeneous lattices should produce Turing patterns and dissipative structures around the bifurcation points, behaviors which will be tracked in the near future.

ACKNOWLEDGMENTS

The authors want to acknowledge the citizens and residents of France, who, by their taxes, made possible the financial support of the Université de Versailles St-Quentin, CNRS, and ANR Agency (BISTA-MAT:ANR-12-BS07-0030-01), who are also acknowledged.

APPENDIX: THE EXPRESSIONS OF α_c^{\pm}

The discriminant D_{λ} , given in Eq. (23), can be factorized under the form $D_{\lambda} = (\alpha - \alpha_c^-)(\alpha - \alpha_c^+)$, where the expressions of the critical values α_c^- and α_c^+ are given by

$$\alpha_c^{\pm} = \Gamma J \frac{\gamma \ln g}{T_{eq}} \left(\frac{T_{eq} + T_B^{\text{crit}}}{2} - T_B \pm \sqrt{(T_{eq} - T_B)^2 - \frac{1}{2}(T_{eq} - T_B)(T_{eq} - T_B^{\text{crit}})} \right). \quad (A1)$$

Both α_c^{\pm} are real, thanks to the condition [Eq. (14)] on the critical bath temperature.

- [1] D. Avnir, M. Kagan, R. Kosloff, and S. Peleg, in *Non-Equilibrium Dynamics in Chemical Systems*, edited by C. Vidal and A. Pacault, Springer Series in Synergetics Vol. 27 (Springer, Berlin, 1984), pp. 118-121.
- [2] G. Nicolis and I. Prigogine, *Self-Organization in Nonequilibrium Systems: From Dissipative Structures to Order through Fluctuations* (Wiley, New York, 1977).
- [3] W. Hordijk and M. Steel, *J. Theor. Biol.* **227**, 451 (2004).
- [4] W. Hordijk, J. Hein, and M. Steel, *Entropy* **12**, 1733 (2010).
- [5] T. A. Lincoln and G. F. Joyce, *Science* **323**, 1229 (2009).
- [6] B. Alberts, A. Johnson, J. Lewis, M. Raff, K. Roberts, and P. Walter, in *Molecular Biology of the Cell*, 4th ed. (Garland Science, New York, 2002), Chap. 6.
- [7] S. K. Scott and K. Showalter, *J. Phys. Chem.* **96**, 8702 (1992).
- [8] J. Jalife, R. A. Gray, G. E. Morley, and J. M. Davidenko, *Chaos* **8**, 79 (1998).
- [9] A. M. Turing, *Philos. Trans. R. Soc. London, Ser. B* **237**, 37 (1952).
- [10] J. F. G. Auchmuty and G. Nicolis, *Bull. Math. Biol.* **38**, 325 (1976).
- [11] P. Bastiaens, M. Caudron, P. Niethammer, and E. Karsenti, *Trends Cell Biol.* **16**, 125 (2006).
- [12] L. Cambi, L. Szego, and A. Cagnasso, *Sci. Fis., Mat. Nat., Rend.* **13**, 809 (1931).
- [13] A. Desaix, O. Roubeau, J. Jeftic, J. Haasnoot, K. Boukheddaden, E. Codjovi, J. Linares, M. Noguès, and F. Varret, *Eur. Phys. J. B* **6**, 183 (1998).
- [14] A. Hauser, *Comments Inorg. Chem.* **17**, 17 (1995).
- [15] A. Slimani, F. Varret, K. Boukheddaden, D. Garrot, H. Oubouchou, and S. Kaizaki, *Phys. Rev. Lett.* **110**, 087208 (2013).
- [16] C. Chong, B. Berini, K. Boukheddaden, E. Codjovi, J. Linars, Y. Garcia, A. D. Naik, and F. Varret, *Physica Status Solidi A* **207**, 1227 (2010).
- [17] B. Viquerat, J. Degert, J. F. Létard, and E. Freysz, *Phys. Rev. B* **87**, 024303 (2013).
- [18] M. Paez-Espejo, M. Sy, F. Varret, and K. Boukheddaden, *Phys. Rev. B* **89**, 024306 (2014).
- [19] F. Varret, M. Paez-Espejo, and K. Boukheddaden, *Europhys. Lett.* **104**, 27003 (2013).
- [20] K. Boukheddaden, I. Shteto, B. Hôo, and F. Varret, *Phys. Rev. B* **62**, 14796 (2000).
- [21] From [20], “the mean-free energy is given by $\mathcal{F}^{\text{hom}} = \frac{1}{2} Jm^2 - k_B T \ln[2g \cosh \beta(Jm - \Delta_{\text{eff}})]$ ”.
- [22] K. Nakano, N. Suemura, S. Kawata, A. Fuyuhiko, T. Yagi, S. Nasu, S. Morimoto, and S. Kaizaki, *Dalton Trans.* (2004) 982.